

## Next-to-leading order gluonic three-jet production at hadron colliders

William B. Kilgore and W. T. Giele

*Fermi National Accelerator Laboratory, P.O. Box 500, Batavia, Illinois 60510*

(Received 23 October 1996)

We report the results of a next-to-leading order event generator of purely gluonic jet production. This calculation is the first step in the construction of a full next-to-leading order calculation of three-jet production at hadron colliders. Several jet algorithms commonly used in experiments are implemented and their numerical stability is investigated. [S0556-2821(97)02711-2]

PACS number(s): 13.87.Ce, 12.38.Bx

### I. INTRODUCTION

In this paper we report the first step in constructing a next-to-leading order (NLO) three-jet event generator for hadron colliders. This involves the construction of the pure gluonic contribution to this cross section. The calculation combines the one-loop virtual matrix elements  $gg \rightarrow ggg$  [1] with the real matrix elements  $gg \rightarrow gggg$  [2–7]. The major issue we want to address in this paper is the convergence and numerical stability of the NLO event generator. The jet algorithm is an integral part of the observed final state and is needed to define the NLO three-jet cross section. Unlike the NLO two-jet calculation, the NLO three-jet calculation is sensitive to many details of the jet algorithm. This is because of the presence of the four-parton final state, which by applying the jet algorithm is converted into either a two-, three-, or four-jet final state. A complete understanding of this partitioning into different numbers of jets requires a careful study of the details of different jet algorithms. For this paper we consider four algorithms: (a) the “fixed-cone” algorithm, used by UA2 [8]; (b) the “iterative-cone” algorithm, used by the Collider Detector at Fermilab (CDF) [9] and D0 Collaborations [10]; (c) the “ $K_T$ ” algorithm [11], under study by CDF and D0 [12]; (d) the “EKS” algorithm, used in NLO one-jet and two-jet inclusive calculations [13].

In Sec. II we will describe the methods and techniques used in the event generator in some detail. Section III describes and investigates the stability of the four-jet algorithms. Some distributions are shown in Sec. IV as an illustration of the achievable numerical accuracy of the event generator. No attempt is made for a detailed phenomenological study; this only makes sense once the quark contributions have been included. Finally, in Sec. V we summarize the findings of the study.

### II. THE METHOD

The construction of a flexible event generator requires the generation of partonic final states with a minimal amount of implicit phase space integration. At leading order (LO) this is trivial, but at NLO it requires careful handling of the cancellation of divergences between the soft and collinear contributions and the virtual corrections. The divergences stem

from the fact that at NLO a parton can only be defined through a resolution criterion. This resolution criterion can take many forms, from a simple invariant mass cut to a full blown fragmentation function. For the studies in this paper a simple invariant mass resolution criterion  $s_{\min}$  suffices. That is, if the invariant mass of two partons is smaller than  $s_{\min}$  they are considered to be unresolvable and treated as a single parton by integrating out the unresolved phase space. This isolates the unresolved soft and collinear regions of phase space from the resolved bremsstrahlung phase space. After this rearrangement, both the resolved contribution and the combination of the unresolved soft and collinear contributions with the virtual corrections are finite [14,15].

With the above method it is easy to calculate the soft and collinear contributions. The next step is to use this calculation to construct a NLO event generator. There are in principle three methods of putting together the resolved partonic cross sections in order to make the NLO jet event generator. In order of complexity they are: (a) “the slicing method,” in which both matrix element and phase space are approximated [16] in the soft and collinear regions, (b) “the subtraction method,” in which the phase space is still approximated in the soft and collinear regions, but the matrix element is now exact (by adding in the correction factor numerically), and (c) “the exact method,” in which both the correction factors for the phase space and matrix elements in the unresolved region are added in numerically. Note that several other methods exist in the literature which are equivalent to method (c) [17]. Method (a) is used to calculate analytically the soft and collinear regions. To be able to perform the integrations and extend the method to arbitrary partonic processes one has to approximate both the matrix element and the phase space in the soft and collinear regions. For any useful and numerically stable event generator method (b) is often sufficient. In a numerical calculation it is trivial to extend method (a) to method (b). Method (c) is attractive because there are no approximations. That is, no terms of order  $s_{\min}$  have been neglected and one can choose the resolution parameter as large as one wants without changing the results. This method, however, is more cumbersome to implement.

One can describe the different methods better using a schematic formula. The  $n$ -parton contribution to the  $(n-1)$ -jet cross section is given by

$$\begin{aligned}
d\sigma_n &= |\mathcal{M}_n|^2 \times J_n dP_n \\
&= [|\mathcal{M}_n|^2 \times (1 - \theta_s) + |\mathcal{M}_n|^2 \times \theta_s] J_n dP_n \\
&= |\mathcal{M}_n|^2 \times (1 - \theta_s) J_n dP_n + \theta_s \times [T_1(\theta_s) + T_2(\theta_s) \\
&\quad + T_3(\theta_s)], \tag{1}
\end{aligned}$$

where the  $n$ -parton differential cross section  $d\sigma_n$  is given by the matrix element squared  $|\mathcal{M}_n|^2$  and the phase space constraints from the jet algorithm and cuts  $J_n$  integrated over the  $n$ -parton phase space  $dP_n$ . The soft or collinear unresolved part of phase space is separated off using the resolution criterion embodied in the quantity  $\theta_s$ , which takes the value  $\theta_s=1$  in the unresolved phase space region and  $\theta_s=0$  otherwise.

$T_1$  is given by

$$\begin{aligned}
T_1(\theta_s) &= S |\mathcal{M}_{n-1}|^2 \times J_{n-1} dP_{\text{soft}} dP_{n-1} \\
&= R(\theta_s) |\mathcal{M}_{n-1}|^2 \times J_{n-1} dP_{n-1}, \tag{2}
\end{aligned}$$

and represents the product of the approximate matrix element  $|\mathcal{M}_n|^2 \rightarrow S |\mathcal{M}_{n-1}|^2$  and the approximate phase space  $dP_n \rightarrow dP_{\text{soft}} dP_{n-1}$ . The resolution factor  $R(\theta_s)$  is independent of the hard scattering and can be integrated analytically for a wide range of multiparton processes [14,15].  $T_2$  is given by

$$T_2(\theta_s) = (|\mathcal{M}_n|^2 - S |\mathcal{M}_{n-1}|^2) J_n dP_n \tag{3}$$

and represents the difference between the true matrix element and the approximate matrix element over the true unresolved phase space.  $T_3$  is given by

$$T_3(\theta_s) = S |\mathcal{M}_{n-1}|^2 (J_n dP_n - J_{n-1} dP_{n-1} dP_{\text{soft}}), \tag{4}$$

and represents the approximate matrix element over the difference between the true unresolved phase space and the approximate unresolved phase space. Note that  $T_1$  contains the soft and collinear divergences needed to cancel the singularities of the virtual term, while  $T_2$  and  $T_3$  vanish as the domain of support for  $\theta_s$  is taken to zero.

Method (a) keeps  $T_1$ , but sets  $T_2=T_3=0$ , method (b) keeps both  $T_1$  and  $T_2$ , but sets  $T_3=0$ , while method (c) keeps all three terms. The terms proportional to the soft factor  $S$  cancel between  $T_2$  and  $T_3$  so that the final expression for method (c) is somewhat simplified. The advantage of method (c) is that the  $\theta_s$  dependence exactly cancels for any value of this resolution parameter. The drawback is that apart from the usual negative weighted virtual plus soft and collinear and positive weighted bremsstrahlung contributions we have now an additional type of negative weighted events which numerically cancel the subtraction term  $R(\theta_s)$ . This can often be confusing, especially when one chooses large values of  $\theta_s$ , because one has a different phase space constraint on this type of bremsstrahlung term. Using method (b) removes these additional events, but now we must choose  $\theta_s$  to be sufficiently small that the phase space approximations are valid. In general this poses no problem and in practice this is the method we use. The effects of the three methods can easily be demonstrated numerically. The  $s_{\min}$

dependence of methods (a) and (b) are shown in Fig. 1 for several jet algorithms. We postpone the discussion of these dependences to Sec. IV.

### III. JET ALGORITHMS

The purpose of the jet algorithm is to quantify certain topological features of hadronic energy flow in scattering processes. By identifying high transverse momentum hadronic clusters in collisions we can make a connection with the underlying partonic scattering and apply perturbative QCD to predict the cross section. The form of the jet algorithm depends to a large extent on the capability of the detector and on the collision environment. Theoretical issues are only of secondary importance. A stable experimental jet algorithm is, by definition, theoretically infrared safe. There are of course issues of perturbative convergence, but the experiment (and implicitly the data) should determine the jet algorithm not vice versa.

With current techniques for theoretical calculations one can easily accommodate any stable experimental jet algorithm. The only crucial theoretical issue is a reliable estimation of the theoretical uncertainties. This is why the NLO predictions for observables are so important. By comparing NLO with LO we can determine the regions of phase space where we can make reliable predictions and give estimates of the uncertainty. There is no point ‘‘improving’’ predictions without a clear understanding of the theoretical uncertainties in the ‘‘improved’’ predictions.

The extension of the NLO two-jet calculation to NLO three jet is nontrivial with respect to the jet algorithm as we will now explain. The algorithms usually depend on a cone-size or distance scale between the clusters:

$$R = \sqrt{(\Delta\eta)^2 + (\Delta\phi)^2}, \tag{5}$$

where  $\Delta\eta$  is the difference in pseudorapidity and  $\Delta\phi$  is the difference in azimuthal angle. When combining clusters of energy one usually follows the ‘‘Snowmass accord’’ [19] which uses transverse energy-weighted ( $E_T$ -weighted) clustering:

$$\begin{aligned}
E_T^{\text{tot}} &= \sum_i E_T^{(i)} \\
\langle \eta \rangle &= \frac{1}{E_T^{\text{tot}}} \sum_i E_T^{(i)} \eta_i \\
\langle \phi \rangle &= \frac{1}{E_T^{\text{tot}}} \sum_i E_T^{(i)} \phi_i.
\end{aligned} \tag{6}$$

We will now summarize our implementations of the four-jet algorithms under consideration.

(a) *The ‘‘fixed-cone’’ algorithm.* This algorithm was used by UA2 and is described in some detail in Ref. [8]. This algorithm is the most basic and straightforward of the four algorithms we are considering. The procedure is very simple.

(1) Form a cluster list, ordering all clusters by  $E_T$ .

(2) Select the highest  $E_T$  cluster from the cluster list and draw a cone of radius  $R$  around the cluster axis. Calculate the

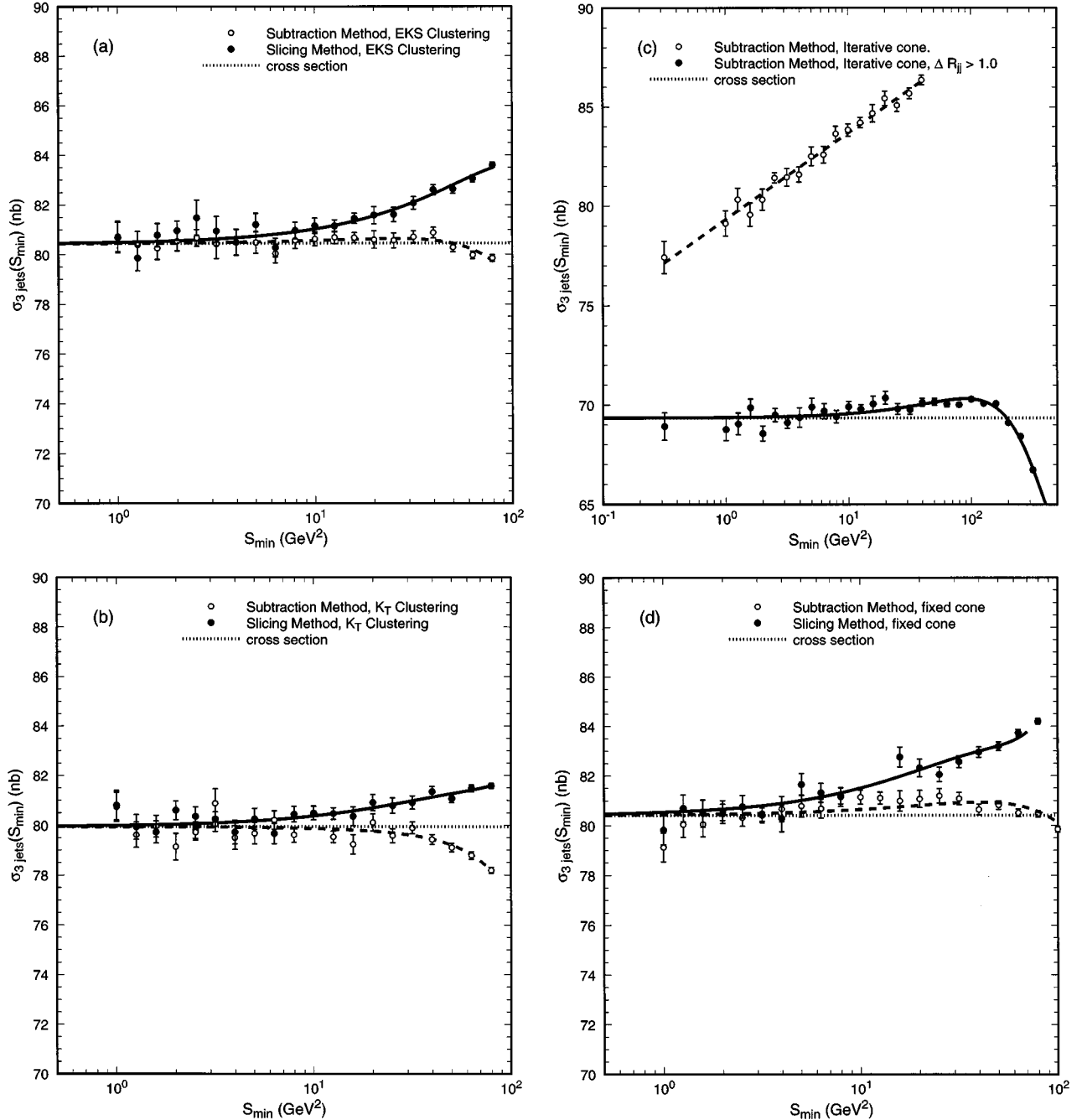


FIG. 1. The  $s_{\min}$ -dependence of the cross section for the different jet algorithms and numerical methods.

transverse jet energy and a new jet axis by performing the  $E_T$ -weighted sum of all the clusters in the cone as defined in Eq. (6).

(3) Remove all clusters in the cone from the cluster list and move the jet to the jet list.

(4) If the cluster list is not empty go to step (2).

(5) Apply the appropriate minimum transverse energy and rapidity cuts to the entries in the jet list to find the final set of jets.

Note that all of the basic physics involved in the clustering is already contained in the three parton final states (i.e., NLO two-jet production or LO three-jet production). No matter how many additional partons are added to the final state, each will be assigned unambiguously to a jet.

(b) *The “iterative-cone” algorithm.* Both CDF and D0 use this algorithm. While it is clearly based on the “fixed-cone” jet algorithm, there are important additions. The algorithm is given by the following.

(1) Form a cluster list, ordered by  $E_T$ .

(2) Select the highest unassigned  $E_T$  cluster, and draw a cone of radius  $R$  around the axis of this cluster. Calculate the transverse jet energy and a new jet axis by merging the clusters in the cone as in Eq. (6).

(3) Draw a new cone around the new jet axis. Recalculate the jet axis using the clusters in the new cone. Repeat this step until a stable jet axis is found.

(4) If there are clusters not yet assigned to at least one jet, go to step (1).

(5) Check for overlapping clusters, i.e., clusters assigned to two or more jets. If overlaps occur, one has to decide whether to merge the jets or to assign the overlapping clusters to separate jets. CDF and D0 have different methods for doing this. CDF merges the jets if any of the overlapping jets shares more than 75% of its  $E_T$ . Otherwise each shared cluster is assigned to the jet to whose axis it is closest in  $\eta$ - $\phi$  space. D0 merges the jets if any jet shares more than 50% of its transverse energy. Otherwise the shared transverse energy is divided equally between the two jets.

(6) Once all clusters have been uniquely assigned to jets, the final jet parameters are calculated, but not using the  $E_T$ -weighted scheme of Eq. (6). For both CDF and D0, the energy and momentum three-vector are calculated by simply adding the four-vectors of the clusters assigned to the jet, and the direction of the jet is given by the sum of the momentum three-vectors. CDF computes the transverse energy of the jet as  $E \sin \theta$ , where  $E$  is the energy calculated above, and  $\theta$  is the polar angle of the jet direction. D0 computes the transverse energy as the scalar sum of the transverse energies of the component clusters. It is worth mentioning that Ref. [18] recently argued that the D0 procedure of defining the final jet parameters leads to large perturbative corrections and therefore should not be used.

(7) Apply the appropriate minimum transverse energy and rapidity cuts to the entries in the jet list to find the final set of jets.

Note that in this case, unlike the ‘‘fixed-cone’’ algorithm, a lot of the physics is missing in the three-parton final state, where there is never an iteration nor is there ever shared energy. To get at all the basic physics one needs at least four parton final states, or in other words NNLO two-jet, NLO three-jet, or LO four-jet production. In fact for NLO two jet and LO three jet the ‘‘iterative-cone’’ algorithm is identical to the ‘‘fixed-cone’’ algorithm.

(c) *The ‘‘EKS’’ algorithm.* The fact that the NLO two-jet calculation does not contain all the needed physics in the jet algorithms used by CDF and D0 inspired the authors of Ref. [13] to introduce an ‘‘improved’’ algorithm which phenomenologically modeled the missing physics. Because this is a theoretical algorithm we will describe it in terms of partons. In NLO two-jet production we have only to consider the three parton final state. The algorithm is then very simple: (1) Consider the possible two-parton configurations by calculating their  $E_T$ -weighted jet axis as if they were clustered; (2) if both partons are within the cone size  $R$  of the hypothetical jet axis they are merged into a single jet; (3) go to step (1) until all two parton configurations have been considered. (4) apply the appropriate minimum transverse energy and rapidity cuts to the entries in the jet list to find the final set of jets.

Note that this maximizes the energy in the cone and simulates the ‘‘iterative-cone’’ algorithm by assuming that it always find the optimum jet axis to maximize the energy in a jet. This in fact overestimates the clustering effects of the ‘‘iterative-cone’’ algorithm. To correct for this an additional parameter called  $R_{\text{sep}}^{(2)}$  was introduced [20]. With this parameter one can impose the additional constraint that only two-parton pairs separated by less than  $R \times R_{\text{sep}}^{(2)}$  can be clustered.

Experimentally it was found that  $R_{\text{sep}}^{(2)} = 1.3$  worked best for  $R = 0.7$  [21]. Note that the quantity  $R_{\text{sep}}^{(2)}$  has no equivalent in experimental jet algorithms and is a purely phenomenological quantity. The  $R_{\text{sep}}^{(2)}$  prescription was tuned to the NLO two-jet calculation, and there are many possible ways to extend it to the NLO three-jet calculation. We choose to do the following.

(1) Consider the possible three-parton configurations by calculating their  $E_T$ -weighted jet axis as if they were clustered. If the three partons are within  $R$  of the hypothetical jet axis and each pair of partons are separated by less than  $R \times R_{\text{sep}}^{(3)}$  they are merged into a single jet. Repeat this step until all three parton configurations have been considered.

(2) Consider the possible two-cluster configurations by calculating their  $E_T$ -weighted jet axis as if they were clustered. If both partons are within  $R$  of the hypothetical jet axis and are separated from one another by less than  $R \times R_{\text{sep}}^{(2)}$  they are merged into a single jet. Repeat this step until all two-cluster configurations have been considered.

It is possible for two two-parton clusters to overlap. These situations are resolved in the following fashion.

(3) If the shared parton contributes more than 75% of the  $E_T$  of either jet, all three partons are merged. If not, the shared parton is assigned to the jet to whose axis it is closest in  $\eta$ - $\phi$  space.

(4) Apply the appropriate minimum transverse energy and rapidity cuts to the entries in the jet list to find the final set of jets.

Note that our implementation of the  $R_{\text{sep}}$  parameters and overlap resolution condition are *ad hoc*, not tuned to the data as  $R_{\text{sep}}^{(2)}$  was for the NLO two-jet calculation. For the NLO three-jet calculation, it could be that  $R_{\text{sep}}^{(3)}$  should take on a different value than  $R_{\text{sep}}^{(2)}$ , that a different overlap resolution prescription will be preferred, or that additional parameters will be needed to accurately describe the data.

(d) *The ‘‘ $K_T$ ’’ algorithm.* This algorithm finds its roots in the  $e^+e^-$  environment. Its adaptation to the  $p\bar{p}$  environment was proposed in Ref. [11]. The algorithm is currently under study in CDF and D0 [12]. Our implementation is based on Ref. [22].

(1) For each cluster  $i$  define a ‘‘closeness’’ to the beam as  $d_{ib} = E_{Ti} R_b$ . For each pair of clusters  $i, j$ , define their closeness to one another as  $d_{ij} = \min\{E_{Ti}, E_{Tj}\} \Delta R_{ij}$ .

(2) Choose the cluster closest to the beam ( $\min\{d_{ib}\}$ ). If  $\min\{d_{ij}\} < d_{ib}$ , merge  $j$  into  $i$ , and remove  $j$  from the cluster list. If all  $d_{ij} > d_{ib}$ , jet  $i$  is said to be ‘‘complete.’’

(3) Go to step (1) until all jets are complete.

(4) Apply the appropriate rapidity and transverse energy cuts to select the final set of jets.

All of the basic physics involved in the  $K_T$  clustering algorithm was already present in the three parton final states. Like the fixed cone algorithm, the  $K_T$  algorithm unambiguously assigns additional partons to jets, no matter how many are added.

The numerical stability of the four jet algorithms is related to the degree to which the algorithm is sensitive to soft radiation, or in other words the infrared stability of the particular algorithm. For the method of resolved partons, as is

used in this paper, infrared stability is related to the extent to which the results are independent of the the resolution parameter  $s_{\min}$ . This dependence is shown in Fig. 1 and will be discussed in the next section.

#### IV. NUMERICAL RESULTS

The calculation presented in this paper includes only the  $gg \rightarrow ggg$  and  $gg \rightarrow gggg$  contribution to the NLO three-jet cross section. This means that any comparison with experimental results would be premature. However, there are several issues we can address in the context of investigating the numerical applicability of the resolved parton approach. First, we can get a first impression of the size of the radiative corrections in the inclusive three-jet cross section by comparing the all-gluon LO three-jet results with the NLO three-jet results. Second, we can start to look at questions related to the jet algorithms and to what extent observables depend on the choice of algorithm. We will look at two particular sets of observables. The first set is the transverse energy distribution of the leading, second, and third jet in the event. The second set involves the transverse energy fraction of the leading, second, and third jet.

For all numerical results in this section we used the CTEQ3M [23] parton distribution functions (PDF's), a fixed renormalization or factorization scale of 100 GeV and a center of mass energy of the  $p\bar{p}$  system equal to 1800 GeV. The fixed scale is needed at NLO because we calculate the gluons-only cross section. The full PDF's, including the quarks, are evolved up to  $Q=100$  GeV. The input gluon PDF is then taken at this scale and not evolved any further (the factorization scale is fixed at 100 GeV). In this manner we get a consistent cross section with only gluons (i.e., taking the number of flavors equal to zero) at NLO. To select events we required at least one jet with  $E_T > 50$  GeV in the rapidity region  $|\eta| < 4$ . Additional jets were required to have  $E_T > 20$  GeV and rapidity in the range  $|\eta| < 4$ . Only events with at least three jets in the final state were selected. The cone sizes were chosen differently per algorithm such that they give approximately the same cross section. The ‘‘iterative-cone’’ algorithm uses the same cone size of 0.7 as is usually chosen experimentally. In the ‘‘EKS’’ algorithm the cone size was chosen to be 0.7 with  $R_{\text{sep}}^{(2)} = R_{\text{sep}}^{(3)} = 1.3$  as is common in the NLO two-jet calculations. In order to accommodate the larger ‘‘effective’’ cone of the two previous algorithms we chose the ‘‘fixed-cone’’ algorithm to have a larger cone,  $R = 0.7 \times 1.3 = 0.91$ . Finally for the ‘‘ $K_T$ ’’-clustering algorithm the closeness parameter is set to  $R_b = 1.0$  (note that this quantity is not really a cone size).

The first issue to be considered is the  $s_{\min}$  dependence of the cross section and the determination of the range in which we can choose its value such that the approximations made in the different numerical methods are valid. The results are shown in Fig. 1 for both the slicing and subtraction method (the exact method has not yet been implemented) and all four types of jet algorithms. The first thing to notice is that the behavior of the iterative cone algorithm is quantitatively different from that of the three other algorithms. The other three algorithms behave as expected and it is clear how to choose  $s_{\min}$  for them. For the slicing method one has to choose  $s_{\min}$  smaller than  $1 \text{ GeV}^2$  in order to get the correct answer.

As expected the subtraction method allows us to choose larger values of  $s_{\min}$ , though the value should still not be larger than  $10 \text{ GeV}^2$ . For the results presented later in this section we will use the subtraction method with  $s_{\min} = 2.5 \text{ GeV}^2$ .

We now consider the iterative cone algorithm. As can be seen in Fig. 1(c), the cross section does not become independent from the resolution parameter, even at very small values of  $s_{\min}$ . In fact the behavior fits very well to a logarithmic dependence on the resolution parameter. This means that the algorithm is not infrared safe in that we can change the jet multiplicity by adding a soft parton somewhere in the event. It is obvious that this can occur when we have three parton configurations in which two of the partons are slightly more than the cone size  $R$  apart balancing the leading third parton. For the tree level and virtual contributions this is a three-jet event. The situation should not change if we add a soft parton in between the two nearby partons, and in fact it does not change for any of the jet algorithms besides the iterative cone. The soft parton gets clustered with one of the hard partons, slightly changing the jet parameters, but not affecting the jet multiplicity. In the case of the iterative cone, however, one of the two hard partons will cluster with the soft parton thereby shifting its jet axis to within  $R$  from the other parton. Because of the iterative nature of this algorithm the two clusters will subsequently be merged further into a single jet yielding a two-jet final state. Thus, we have changed the jet multiplicity by adding an arbitrarily soft parton to the event. As a result the algorithm is infrared unstable and cannot be used within the context of perturbative QCD. Experimentally this means that the jet algorithm depends on the implicit soft cutoffs in the detector, e.g., granularity of the detector, cluster cutoff, and ultimately hadron masses. In other words, the jet multiplicity depends on the ability of the detector to resolve and measure soft hadrons. It is clear that we cannot use this algorithm within the NLO calculation. Note that this result does not make the one- and two-jet inclusive cross sections infrared unstable since in those cases we do not have to resolve three-jet configurations. Both CDF and D0 have compared their multijet data (i.e., more than two jets in the final state) with LO Monte Carlos [10,24]. It is interesting to note that the experiments have in fact added an additional cut to their multijet cross section in order to make these comparisons. This cut requires all the jets in the event to be further apart than their cone size of  $R=0.7$ . For CDF this cut was  $\Delta R_{jj} > 1.0$ , while for D0 the requirement is  $\Delta R_{jj} > 1.4$ . This additional requirement in the jet algorithm changes the  $s_{\min}$  dependence of the cross section dramatically, as can be seen clearly in Fig. 1(c). In fact the behavior is now very similar to the other three algorithms. This is no surprise since with this additional selection cut the infrared instability is removed. This means that the iterative cone algorithm needs to be augmented with a jet separation cut in order to be an infrared safe jet algorithm.

The most basic distributions we can look at are the  $E_T$ -ordered transverse energy distributions. These distributions are given in Fig. 2 for various jet algorithms. The curves are fits to Monte Carlo output and have a fit uncertainty associated with them. The fit uncertainty for the leading jet is shown in Fig. 2(d) where the leading jet  $K$  factor (i.e., the ratio of NLO over LO) is given together with the 1-

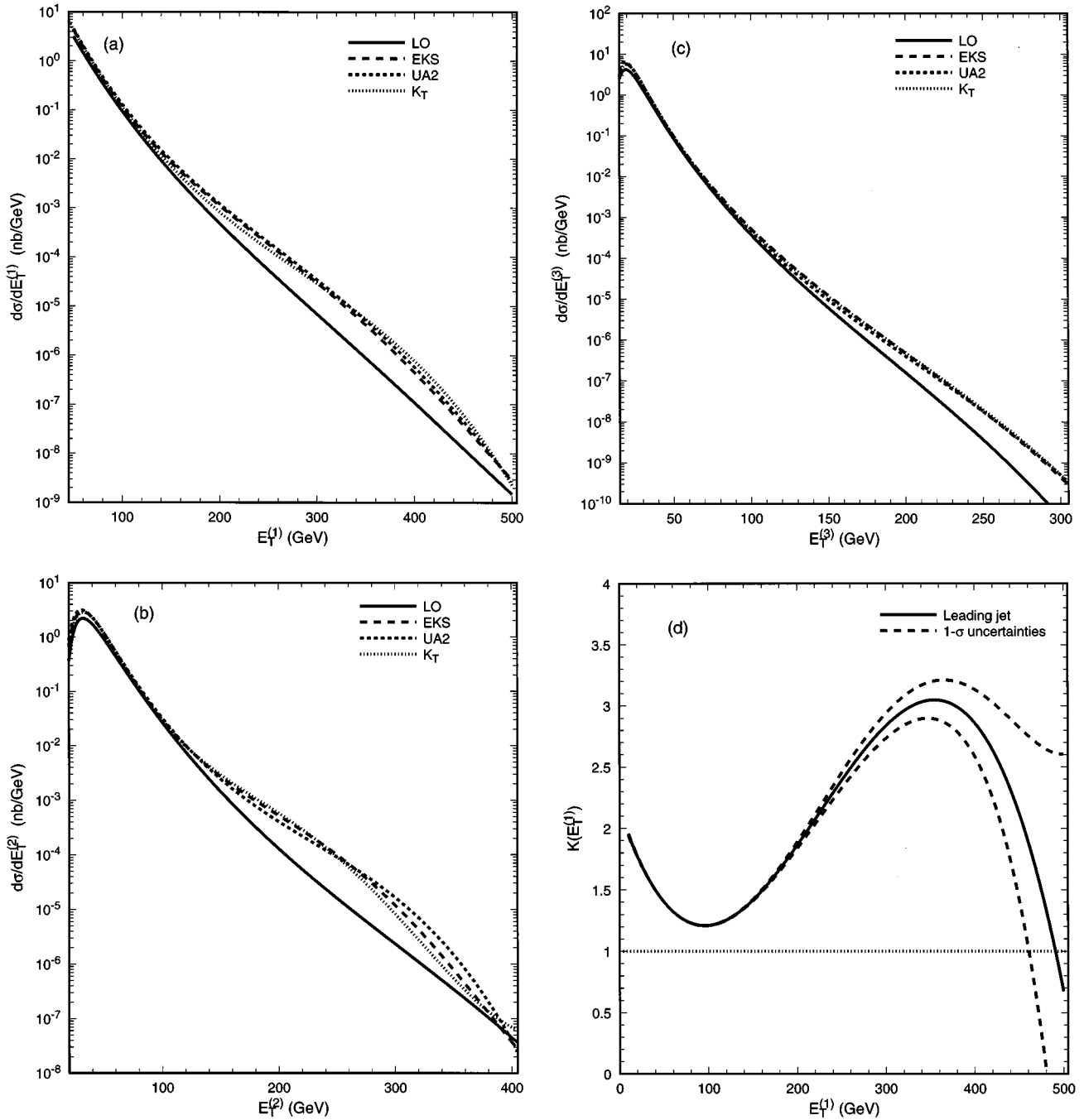


FIG. 2. The  $E_T$  spectra of the (a) leading, (b) second, and (c) third jet. (d) contains the  $K$  factor of the leading jet for the EKS clustering scheme.

$\sigma$  boundary on the fit. The uncertainties on the second and third jet are very similar in size and  $E_T$  dependence. As can be seen from Figs. 2(a), 2(b), and 2(c) the differences between the jet algorithms are small and stable, especially when taking the fit uncertainties into account. The LO normalization is highly uncertain because it is an  $\alpha_S^3$  process and therefore very dependent on the value of  $\alpha_S$  (i.e., at LO the renormalization scale choice). The radiative corrections, however, show more structure than a simple normalization shift. The radiative effects can be quite substantial, with a  $K$  factor as large as 3 for  $E_T=350$  GeV. There are two reasons for these large corrections. Note that the minimum in the  $K$  factor for leading jet occurs at  $E_T=100$  GeV, exactly

at the renormalization or factorization scale choice. This is no accident. Usually one would choose this scale to be equal or proportional to the leading jet  $E_T$ . For the gluons-only process, however, this would require evolving the PDF's with  $n_f=0$ . So, part of the large corrections away from  $E_T=100$  GeV are due to the choice of renormalization or factorization scale which generates large logarithmic corrections at higher orders. The second reason is that we look at gluons only, while evolving the PDF's to a scale of 100 GeV using both quarks and gluons. This means the gluon content of the proton and therefore the size of the radiative corrections in the gluons-only case depend on the mass factorization scheme used in the PDF and matrix element. Any

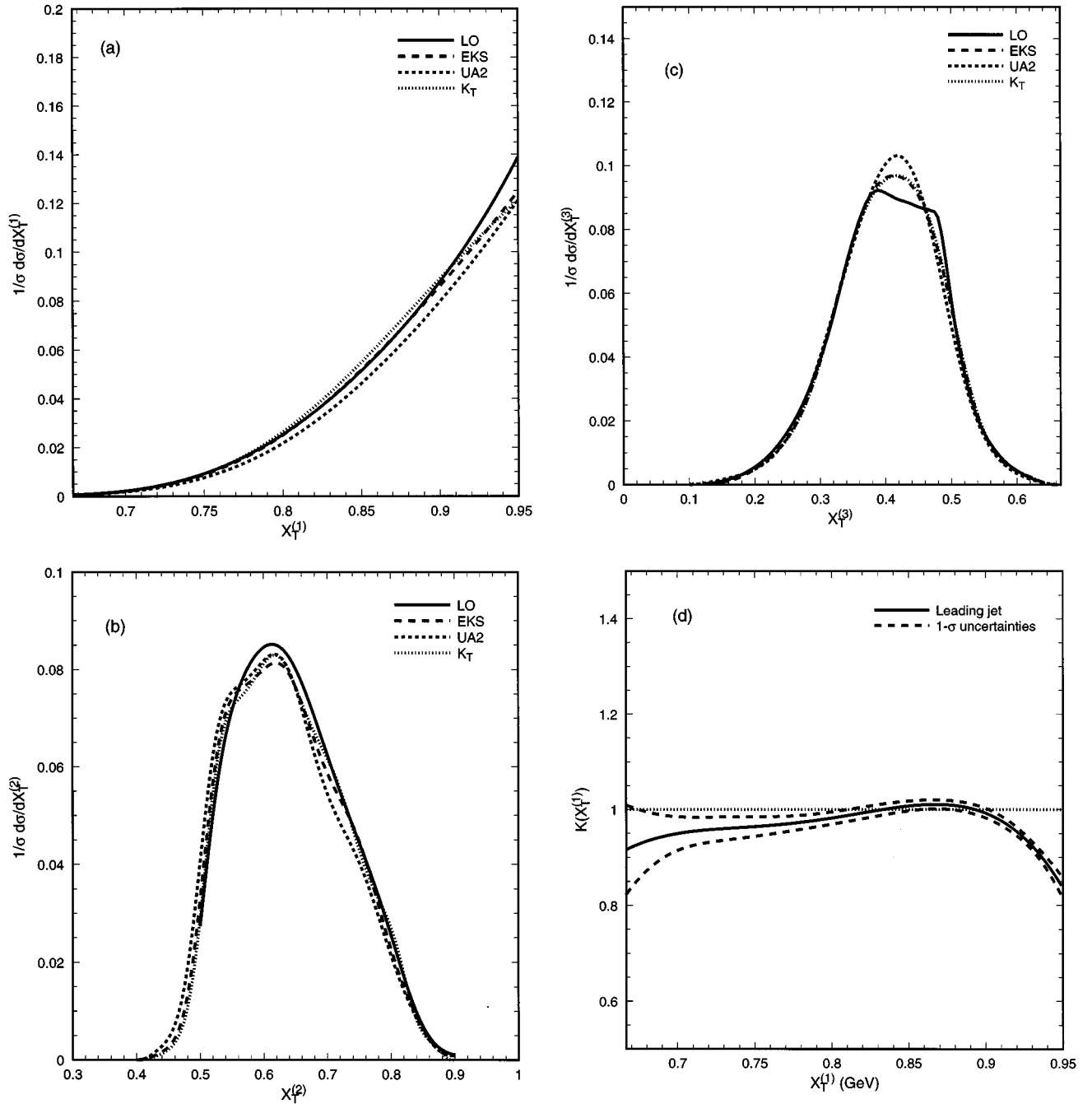


FIG. 3. The  $X_T$  spectra of the (a) leading, (b) second, and (c) third jet and (d) the  $K$  factor for the leading jet as a function of  $X_T$ .

conclusion on the radiative corrections in the full case (i.e., including the quark processes) is therefore premature. Note that in the modified minimal subtraction ( $\overline{\text{MS}}$ ) scheme used in this calculation the contribution of gluon initiated scattering at  $E_T=350$  GeV is very small. The scattering at such large momentum transfers is dominated by  $t$ -channel quark scattering, making the size of the gluons-only  $K$  factor irrelevant.

The final observable we will look at in our investigation of the stability of the NLO three-jet event generator is the transverse energy fraction  $X_T^{(i)} = 2E_T^{(i)}/\sum_{j=1}^3 E_T^{(j)}$  of the three leading jets (in transverse energy) in the event. These are different from the usual observables used by the experimentalists (see, e.g., the CDF papers [9,24]). They look at the

energy fraction  $X^{(i)} = 2E^{(i)}/M_{jjj}$  where the energies are defined in the center-of-mass frame of the collision and  $M_{jjj}$  is the invariant mass of the three leading jets. We have chosen the transverse energy fractions because they do not require the determination of the center-of-mass reference frame. At NLO, the determination of the center-of-mass frame is strongly dependent on the ability to detect forward radiation, making the NLO prediction rather unstable and detector dependent. The transverse energy fraction, on the other hand, behaves more stably and radiative effects are small. This can be seen in Fig. 3 where the normalized LO and NLO transverse energy fraction distributions are plotted for several jet algorithms. Also shown is the  $K$  factor for the normalized  $X_T^{(1)}$  distribution together with its fit uncertainties. The radi-

tive corrections for these distributions are in general small, except at the edge of LO phase space where the jet algorithm sensitivity also becomes large. (At LO the transverse energy fractions are constrained to  $2/3 < X_T^{(1)} < 1$ ,  $1/2 < X_T^{(2)} < 1$ , and  $0 < X_T^{(3)} < 2/3$ , not taking any  $E_T$  cuts into account.) The NLO three-jet event generator is capable of predicting these distributions accurately enough for comparisons with experiments.

## V. CONCLUSIONS

In this paper we have presented results on the purely gluonic contribution to the NLO three-jet cross section. All of the techniques used can be readily applied to the quark contributions. Several techniques to isolate the soft or collinear contributions were explored and their numerical effects investigated.

All of the relevant experimental jet algorithms were implemented in the NLO three-jet event generator and their radiative effects studied. For the iterative cone algorithm it was necessary to augment the algorithm with an additional jet separation cut in order to obtain infrared stability. Both CDF and D0 already apply such a cut in their multijet analy-

sis, though the reason is the inefficiency of the cluster algorithm instead of the theoretically motivated removal of the infrared instability. The other jet algorithms behaved properly and no additional cuts were needed.

The NLO three-jet event generator was applied to several distributions and it was demonstrated that one could obtain useful results which can be compared to the experimental data, once the quark matrix elements are included.

Note added: After this work was completed, we learned of a similar calculation by Z. Trócsányi [25].

## ACKNOWLEDGMENTS

We would like to thank the Fermilab lattice QCD group for the kind use of the ACPMAPS supercomputer, on which the calculations in this paper were performed, and George Hockney for his assistance in using it. We would like to thank Lance Dixon for comparing our numerical implementation of the matrix elements in Ref. [1] to the authors' results. Fermilab is operated by Universities Research Association, Inc., under Contract No. DE-AC02-76CH03000 with the U.S. Department of Energy.

- 
- [1] Z. Bern, L. Dixon, and D.A. Kosower, Phys. Rev. Lett. **70**, 2677 (1993).
  - [2] S. Parke and T. Taylor, Nucl. Phys. **B269**, 410 (1986).
  - [3] Z. Kunszt, Nucl. Phys. **B271**, 333 (1986).
  - [4] J. Gunion and J. Kalinowski, Phys. Rev. D **34**, 2119 (1986).
  - [5] F.A. Berends and W.T. Giele, Nucl. Phys. **B294**, 700 (1987); **B306**, 759 (1988).
  - [6] M. Mangano, S. Parke, and Z. Xu, *Proceedings of Results and Perspectives in Particle Physics*, edited by M. Greco (Editions Frontières, Gif-sur-Yvette, 1987), p. 513; M. Mangano, S. Parke, and Z. Xu, Nucl. Phys. **B298**, 653 (1988).
  - [7] M. Mangano and S. Parke, Phys. Rep. **200**, 301 (1991).
  - [8] UA2 Collaboration, J. Alitti *et al.*, Phys. Lett. B **257**, 232 (1991).
  - [9] CDF Collaboration, F. Abe *et al.*, Phys. Rev. D **45**, 1448 (1992).
  - [10] D0 Collaboration, S. Abachi *et al.*, Phys. Rev. D **53**, 6000 (1996).
  - [11] S. Catani, Y.L. Dokshitzer, and B.R. Webber, Phys. Lett. B **285**, 291 (1992); S.D. Ellis and D.E. Soper, Phys. Rev. D **48**, 3160 (1993).
  - [12] D0 Collaboration, spokesperson, K.C. Frame, *Proceedings of the 8th Meeting of the Division of Particles and Fields of the American Physical Society*, edited by S. Seidel (World Scientific, Singapore, 1995), p. 1650.
  - [13] S.D. Ellis, Z. Kunszt, and D.E. Soper, Phys. Rev. Lett. **62**, 726 (1989).
  - [14] W.T. Giele and E.W.N. Glover, Phys. Rev. D **46**, 1980 (1992).
  - [15] W.T. Giele, E.W.N. Glover, and D.A. Kosower, Nucl. Phys. **B403**, 633 (1993).
  - [16] H. Baer, J. Ohnemus, and J.F. Owens, Phys. Rev. D **40**, 2844 (1989).
  - [17] Z. Kunszt and D.E. Soper, Phys. Rev. D **46**, 192 (1992); S. Catani and M.H. Seymour, Phys. Lett. B **378**, 287 (1996); S. Frixione, Z. Kunszt, and A. Signer, Nucl. Phys. **B467**, 399 (1996).
  - [18] E.W.N. Glover and D.A. Kosower, Phys. Lett. B **367**, 369 (1996).
  - [19] J. E. Huth *et al.*, in *Proceedings of the 1990 Summer Study on High Energy Physics*, edited by E. L. Berger (World Scientific, Singapore, 1992), p. 134.
  - [20] S.D. Ellis, Z. Kunszt, and D.E. Soper, Phys. Rev. Lett. **69**, 3615 (1992).
  - [21] CDF Collaboration, F. Abe *et al.*, Phys. Rev. Lett. **70**, 713 (1993).
  - [22] M.H. Seymour, in *Proceedings of the 10th Topical Workshop on Proton-Antiproton Collider Physics*, edited by R. Raja and J. Yoh (AIP Press, Woodbury, NY, 1996), p. 568.
  - [23] CTEQ Collaboration, H.L. Lai *et al.*, Phys. Rev. D **51**, 4763 (1995).
  - [24] CDF Collaboration, F. Abe *et al.*, Phys. Rev. D **54**, 4221 (1996).
  - [25] Z. Trócsányi, Phys. Rev. Lett. **77**, 2182 (1996).